Mining, Metallurgy & Exploration (2021) 38:1525–1535
https://doi.org/10.1007/s42461-021-00412-z

A Hydrometallurgical Approach to Produce Nano-ZnO from Electrical Arc Furnace Dusts

Esmaeel Darezereshki[1] · Ali Behrad Vakylabad[2] · Babak Koohestani[3]

Received: 7 June 2020 / Accepted: 19 February 2021 / Published online: 10 March 2021

Abstract

As a by-product of the steelmaking industry rich in iron and zinc, electric arc furnace dust (EAFD) landfill disposal is restricted in many countries due to the metal lixiviation risks. Several approaches have been examined to recycle or reuse EAFD. Hydrometallurgical methods mainly include the preparation of pregnant acid leached solution (PLS) using inorganic acids followed by selective metal recovery using different methods. We herein proposed a hydrometallurgical process initiated by acid leaching and finalized by thermal treatment to produce nano-ZnO from EAFD. At the condition of this study, only 67% of zinc was leached by sulfuric acid from EAFD into PLS while 98% of surplus leached iron was removed through precipitation by sodium hydroxide. Additional purification of iron removed PLS was accomplished using di-2 ethylhexyl phosphoric acid to extract Zn^{+2}. The addition of ammonium hydroxide to purified PLS provided $(Zn(OH)_2)_3(ZnSO_4)(H_2O)_5$ as the final precursor for nano-ZnO that ultimately transformed to nano-ZnO (60 ± 6 nm particle size) at 850 °C. The achieved results were scrutinized through various tests and analyses including TEM, XRD, SEM, EDS, FTIR, and TGA.

Keywords Electric arc furnace dust · Leaching · Purification · Nanoparticle · ZnO

1 Introduction

Electric arc furnace dust (EAFD) as a by-product of steel accounts for 60% of generated waste in steelmaking industries. Since containing heavy metals (e.g., Fe, Zn, Pb, Cd, Cr), the landfill storage of EAFD is restricted because of metal lixiviation risk [4, 16, 19, 22, 24, 29, 32, 42]. In this case, EAFD management requires an enclosed well-monitored costly in- and output systems [24]; the management costs of EAFD in Iran, for example, (solidification or stabilization) exceeds 180 $/t. Depending on the ratio of galvanized scrap utilized, zinc content in EAFD fluctuates between 7 and 40% that can represent an annual zinc production of 0.5–2 tons. Due to the increasing price and various usages, zinc recovery from EAFD is legitimate to work on [31].

Pyrometallurgical and hydrometallurgical methods or a combination of both are considered as the main recycling approaches to recover valuable materials from a mixture [11, 41, 44]. Hydrometallurgical recycling techniques are more advantageous over pyrometallurgical approaches since being more tolerable to recover low-grade elements and remove impurities [3, 14, 19, 22, 27, 30, 41, 42]. The main challenge in the hydrometallurgical recovery of zinc is to increase the recovery level, particularly in low-grade zinc EAFD. The most well-known EAFD leaching reagents include inorganic acids (e.g., H_2SO_4, HCl, HNO_3), organic acids (e.g., $C_6H_8O_7$), and bases (e.g., NaOH) [10, 15] among which hydrochloric acid and aqua regia displayed higher recovery rate with a minor iron release [11]. After preparation of pregnant leach solution (PLS) from the acid leaching process, different methods can be applied to recover metals such as precipitation [35, 41], crystallization [26, 35], solvent extraction [1, 35], ion exchange [18], and electrowinning [35].

Due to the superior properties, nano-ZnO structures can be used in several applications including electronic sensors, solar voltaic, transducer, batteries, antimicrobial products, and lubricants [21, 25, 45]. Different approaches have been taken to

✉ Esmaeel Darezereshki
darezereshki@uk.ac.ir

✉ Ali Behrad Vakylabad
alibehzad86@yahoo.co.uk; a.behrad@kgut.ac.ir

[1] Department of Materials Engineering, Shahid Bahonar University, P. O. Box 76169-133, Kerman, Iran

[2] Department of Materials, Institute of Science and High Technology and Environmental Sciences, Graduate University of Advanced Technology, 76315-117, Kerman, Iran

[3] Mining and Mineral Processing Department, Tarbiat Modares University, Tehran, Iran

Table 1 XRF microanalysis of EAFD

Oxides Wt%	Fe_2O_3	ZnO	CaO	SiO_2	MgO	Cl	MnO	PbO	Na_2O	K_2O	CuO	Cr_2O_3	SO_3	P_2O_5	Co_3O_4	Al_2O_3
	42.2	22.9	11.2	3.5	3.3	3.9	2	1.4	2.7	2.8	0.36	0.33	2.2	0.24	0.026	0.93

fabricate nano-ZnO structures such as alkali-precipitation, thermal decomposition, hydrothermal synthesis, colloidal chemistry, and emulsion, sol–gel [9, 12, 13, 34]. Recently, the synthesis of nano-ZnO particles from leached EAFD has been practiced as a new waste management and recycling approach [33, 38, 43]. In general, hydrometallurgical methods containing wet chemicals followed by thermal treatments are recommended to fabricate nanoparticles since being simple, flexible, cheap, and less dependent on advanced equipment.

This study applies the same approach as the authors were previously taken to fabricate nano-ZnO from zinc sulfate solution ($ZnSO_4{\cdot}7H_2O$) [6]. However, the source and composition of PLS in this study were EAFD and $(Zn(OH)_2)_3(ZnSO_4)(H_2O)_5$. Thus, a modified hydrometallurgical approach combined with thermal treatment was proposed to assemble nano-ZnO from EAFD while the role of iron impurity was negligible.

2 Materials and Methods

2.1 Materials

The EAFD samples were provided by the Iranian National science foundation (under contract No. 90003855, Appendix) from the dust collectors of Iranian Alloy-Steelmaking in Yazd. The chemical composition and mineralogical phases of EAFD were estimated using X-ray fluorescence (XRF, PANalytical AXIOS XRF spectrometer) and X-ray diffraction (XRD, PHILIPS, X' pert-MPD, Cu Kα (λ = 1.54 Å), 40 kV, 30 mA, 10° to 80°, 3°/min). Table 1 and Fig. 1 present XRF and XRD results of the EAFD sample used in this study. As can be seen from Table 1 and Fig. 1, the provided EAFD contains moderate zinc level while the main mineralogical compositions are composed of ZnO, $ZnFe_2O_4$, $FeFe_2O_4$, Fe_2O_3, SiO_2, and $Ca(OH)_2$ [23]. Figure 2 displays the particle size distribution (PSD) of EAFD specimen using Malvern Mastersizer-S laser scattering analyzer (NICOMP 370, USA) while the d_{50} and d_{90} particle sizes fluctuate between − 2 and − 18 μm.

The pure analytical materials used in this experimental study are sulfuric acid (H_2SO_4, 99%, Merck), sodium hydroxide (NaOH, 99%, Merck), ammonium hydroxide (NH_4OH, 99%, Merck), LIX 84I (2-hydroxy-5-nonylacetophenone oxime), D2HEPA (di(2-Ethylhexyl) phosphoric acid, 97%, Sigma-Aldrich), de-ionized water, and ethanol (CH_3CH_2OH) were purchased and used as pure analytical reagents.

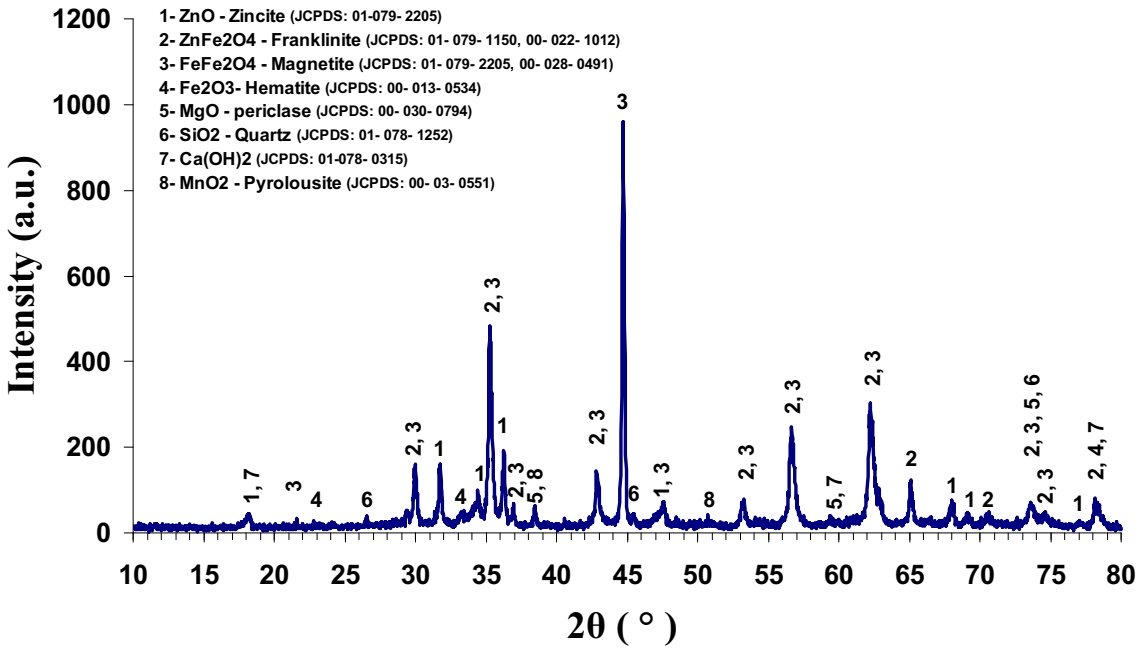

Fig. 1 X-ray diffraction showing mineralogical phases of the EAFD

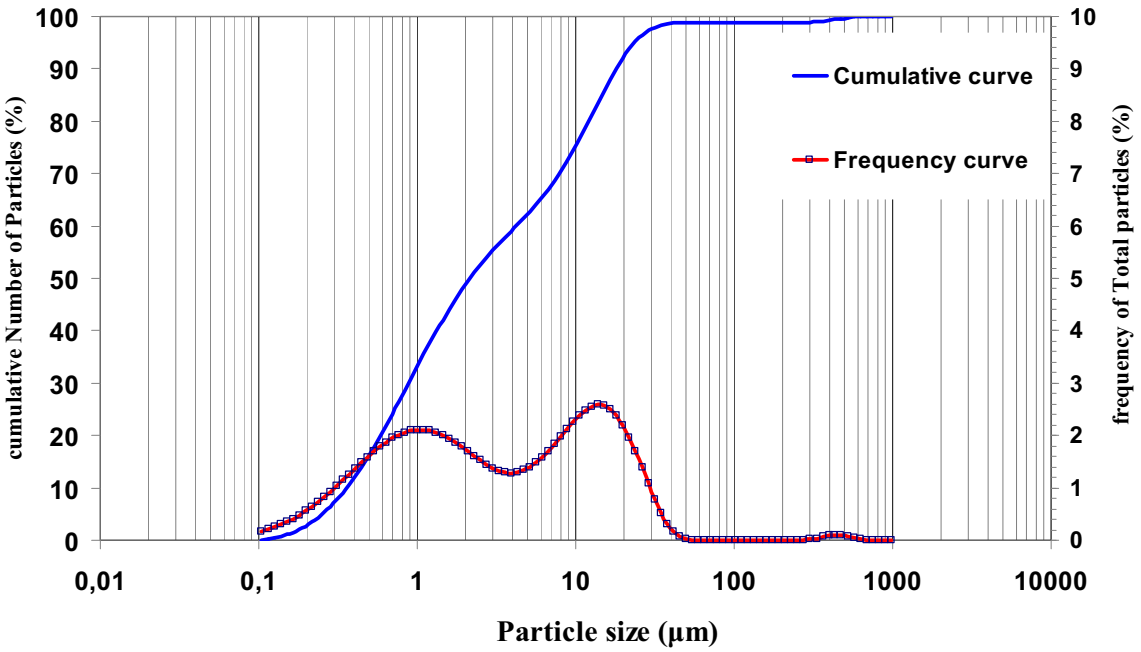

Fig. 2 Particle size distributions of the starting EAFD

2.2 Experimental Methods

The experimental methods start with the preparation of PLS containing zinc sulfate from EAFD using diluted sulfuric acid as the lixiviant. Sodium hydroxide was also used to separate iron from zinc ions. In the final stage before thermal treatment, ammonium hydroxide reduction agent was used to prepare Nano-ZnO. The morphology and chemical composition of the precursor (sulfo-hydro-zincite) and as-prepared nano-ZnO were determined by scanning electron microscope (SEM, Tescan Vega-II) equipped with an energy dispersive spectroscope (EDS). The detailed morphology of nanoparticles was also evaluated using a Transmission Electron Microscope (TEM, PHILIPS CM20) operated at 20 kV. The elemental composition of the pregnant leach solution was also evaluated using atomic absorption spectroscopy (AAS, Perkin Elmer 4100) and ICP-MS (ICP-MS, X Series II, Thermo Scientific). In addition, iron (Fe^{2+} and Fe^{3+}) analysis was conducted by back-titration using potassium dichromate ($K_2Cr_2O_7$). To understand and compare the surface chemistry of precursor and nanoparticles, Fourier-transform infrared (FTIR) spectrometer was performed with KBr pellet on a Bruker tensor 27 using RT-DLATGS detector in the range of 400–4000 cm^{-1} with spectral resolution of 4 cm^{-1} in transmittance mode. Thermogravimetry/differential scanning calorimetry (TG/DSC) test was performed (STA409PG) under N_2 flow, a heating rate of 10 °C/min up to 1200 °C. The aim was to

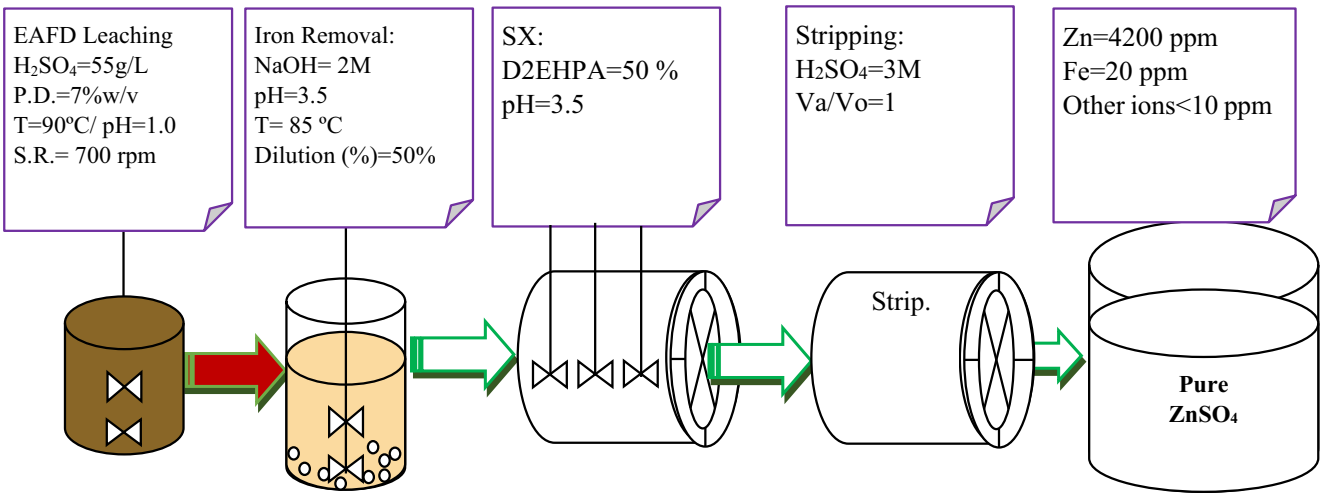

Fig. 3 Pure $ZnSO_4$ solution preparation from EAFD using D2HEPA

Table 2 Elemental compositions of original and iron removed PLS using NaOH

Element	Cd	Co	Cr	Cu	Fe	Ni	Zn
PLS (ppm)	29.87	<0.05	<0.05	160.78	11191	4.82	8562
Purified PLS (pms)	15.73	<0.05	<0.05	63.36	90	2.16	4195

study the thermal decomposition temperature of impurities in the precursor of nano-ZnO (e.g., sulfates) [31, 40].

3 Results and Discussion

3.1 Leaching and Purification

Figure 3 displays the EAFD leaching process that ends with $ZnSO_4$ preparation. High-level calcium bearing or metal oxide minerals (e.g., CaO, Fe_2O_3) increase the acid consumption level during the leaching process [36]. Based on the obtained results, the leaching process at 90 °C reduced the acid consumption and minimized the iron release into the PLS while the maximum zinc recovery (67%) took place at pH = 1.0, 3 M H_2SO_4, 7% pulp density (P.D., w/v), and stirring rate (S.R.) of 700 rpm. As can be seen from Table 2, a considerable amount of iron as an impurity was leached to PLS that needs to be removed. To eliminate iron from PLS and initiate the formation of $ZnSO_4$ solution, two reagents including jarosite and sodium hydroxide are proposed [37]. However, sodium hydroxide was more efficient to remove iron (up to 98%) through precipitation at pH=3.5, 50% diluted PLS, and T= 85 °C. Table 2 displays the ICP-MS analysis of the PLS before and after iron removal. Selective extract of Zn^{2+} from iron removed PLS was performed using two chemical reagents including LIX 84I and D2HEPA while D2EHPA resulted in a higher recovery rate (98.5%) at pH = 3.5, 20% D2HEPA/80% Kerosene, and V_o/V_a = 1. However, using LIX 84I reagent to extract Zn^{2+} at pH = 9, 20% LIX 84I/80% Kerosene, and V_o/V_a = 1 resulted in 84% zinc recovery only. In the stripping step, the recovered Zn^{2+} exposed to 3 M H_2SO_4 solution to prepare pure $ZnSO_4$ solution for the generation of nano-ZnO.

3.2 Production of Nano-ZnO

Figure 4 displays the chemical procedure of nano-ZnO production used in this research study. The prepared high concentration $ZnSO_4$ solution from the leaching section was diluted in 0.5 M H_2SO_4 solution to be prepared for the generation of nanoparticles [6]. The 0.5 M Zn^{2+} solution was introduced into a reactor with NH_4OH dropping onto the solution with vigorous stirring at 70 °C for 50 min until a white zinc hydroxy sulfate complex, $(Zn(OH)_2)_3(ZnSO_4)(H_2O)_5$, precipitates. Thereafter, the precipitated complex precursor was filtered, rinsed with deionized water and ethanol, dried at 70 °C for 24 h, and finally calcinated in a muffle furnace at 850 °C for 1 h to prepare the final nano-ZnO. Table 3 displays the overall leaching efficiency of EAFD for the fabrication of nano-ZnO as the final product. To evaluate the efficiency of the method in the transformation of released zinc from acid leached EAFD to nano-ZnO, the mass balance was calculated using the following general formula [20]:

$$\gamma_i = \frac{(C_i \times V)}{(m_0 \times w_0)} \times 100\%$$

in which

C_i the concentration of species (i)
V the volume of aqueous leaching solution
m_0 the mass of the feed or starting materials
w_0 the compositions of species (i)

In this case, the total zinc in leaching stage equals to 500 ml × 7% (w/v) × 18.4% = 6.44 g that provides maximum zinc leach recovery of 6.44 g × 67% = 4.34 g. At the same time, the total zinc in the diluted PLS was 4.12 g (1 M Zn^{2+} = 65.41 g/L) obtained from the stripping solution with 3 M H_2SO_4 = 29 g/L Zn^{2+}. With 98.5% recovery rate of Zn^{2+} about 4.06 g of

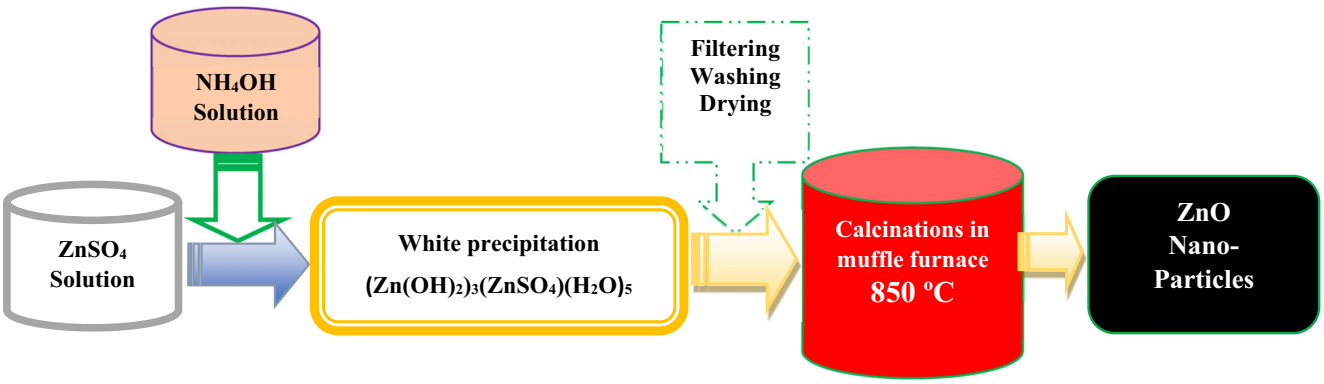

Fig. 4 Flowsheet of nano-ZnO produced from $ZnSO_4$ solution

Table 3 Mass balance of leached zinc from the EAFD to the final product, nano-ZnO powder

Zn in EAFD (%)	18.4
Beaker volume (mL)	500
Total zinc in leaching stage (g)	6.44
Optimum zinc recovered (g)	4.34
Total zinc in the diluted PLS (g)	4.12
Recovery rate of Zn^{2+} (%)	98.5
Total zinc transferred into the stripping solution (g)	4.06
stripping solution characteristic	3 M H_2SO_4; 29 g/L Zn^{2+}
Total precipitation yield (%)	96.72
Total Zn recovered as ZnO (g)	3.93
Total efficiency of the project (%)	61.00

the leached zinc was transferred into the stripping solution in each SX cycle. Similarly, these calculations were performed for all operational steps to complete Table 3.

3.3 Characterization of Nano-ZnO

3.3.1 Thermogravimetric Analysis (TG/DSC)

Regarding the fact that various intermediates have different thermal decomposition temperatures the plotted TG/DSC curves in Fig. 5 present four major weight loss in the precursor of nano-ZnO or $(Zn(OH)_2)_3(ZnSO_4)(H_2O)_5$ [39, 40].

Equations 1–3 propose the chemical reaction of the precursor during thermal treatment. The first weight loss at approximately 100 °C indicates the evaporation of free water from the sample. The second weight loss between 200 and 300 °C is related to the mineralogical chemisorbed water removal. Small fluctuations of the DSC curve from 450 to 520 °C may present the mineralogical alteration of the specimen. A total weight loss of 25.9 wt.% observed in the TG curve corresponds to the theoretical weight loss of $(Zn(OH)_2)_3(ZnSO_4)(H_2O)_5$ to zinc oxide. As such, pure ZnO nanoparticles could be obtained at 850 °C through calcining the intermediate precursor [6].

$$\left(Zn(OH)_2\right)_3(ZnSO_4)(H_2O)_5 \rightarrow ZnSO_4.3Zn(OH)_2 + 5\,H_2O \quad (1)$$

$$2\left[ZnSO_4.3Zn(OH)_2\right] \rightarrow 5ZnO + Zn_3O(SO_4)_2 + 6H_2O \quad (2)$$

$$Zn_3O(SO_4)_2 \rightarrow 3ZnO + 2SO_2 + O_2 \quad (3)$$

3.3.2 Morphological and Elemental Study

Figures 6a–c display SEM photomicrograph of unannealed pellet of $(Zn(OH)_2)_3(ZnSO_4)(H_2O)_5$ precursor while Fig. 6b shows agglomerated as-synthesized ZnO nanoparticles. EDS spectrum (Fig. 6d) displays the existence of zinc and oxygen ions only as the indicators of pure zinc oxide that legitimates the proposed calcination temperature. The obtained Zn/O atomic weight ratio out of the EDS profiles of as-

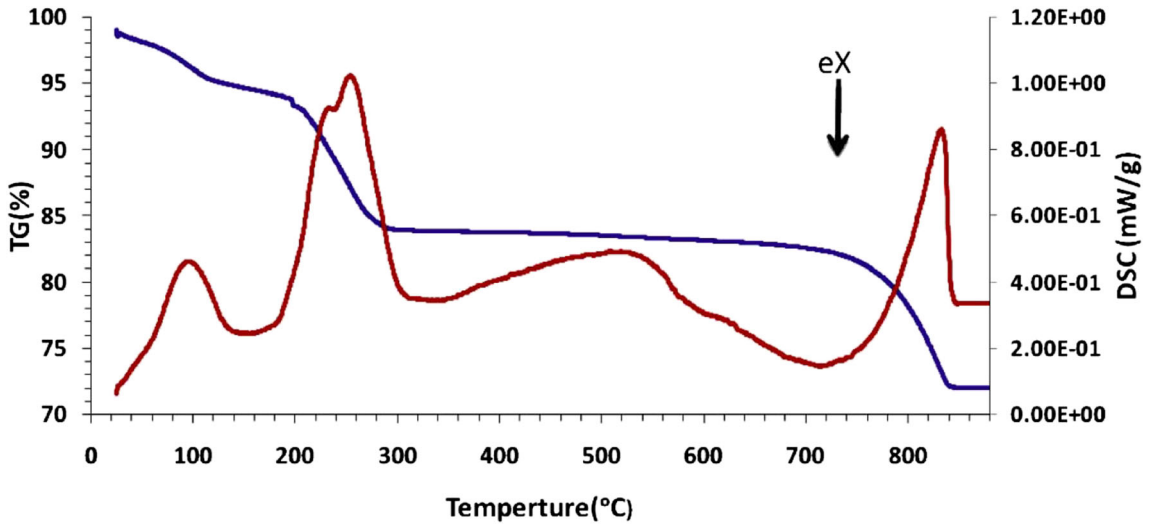

Fig. 5 TG/DSC curves for pure precursor of nano-ZnO

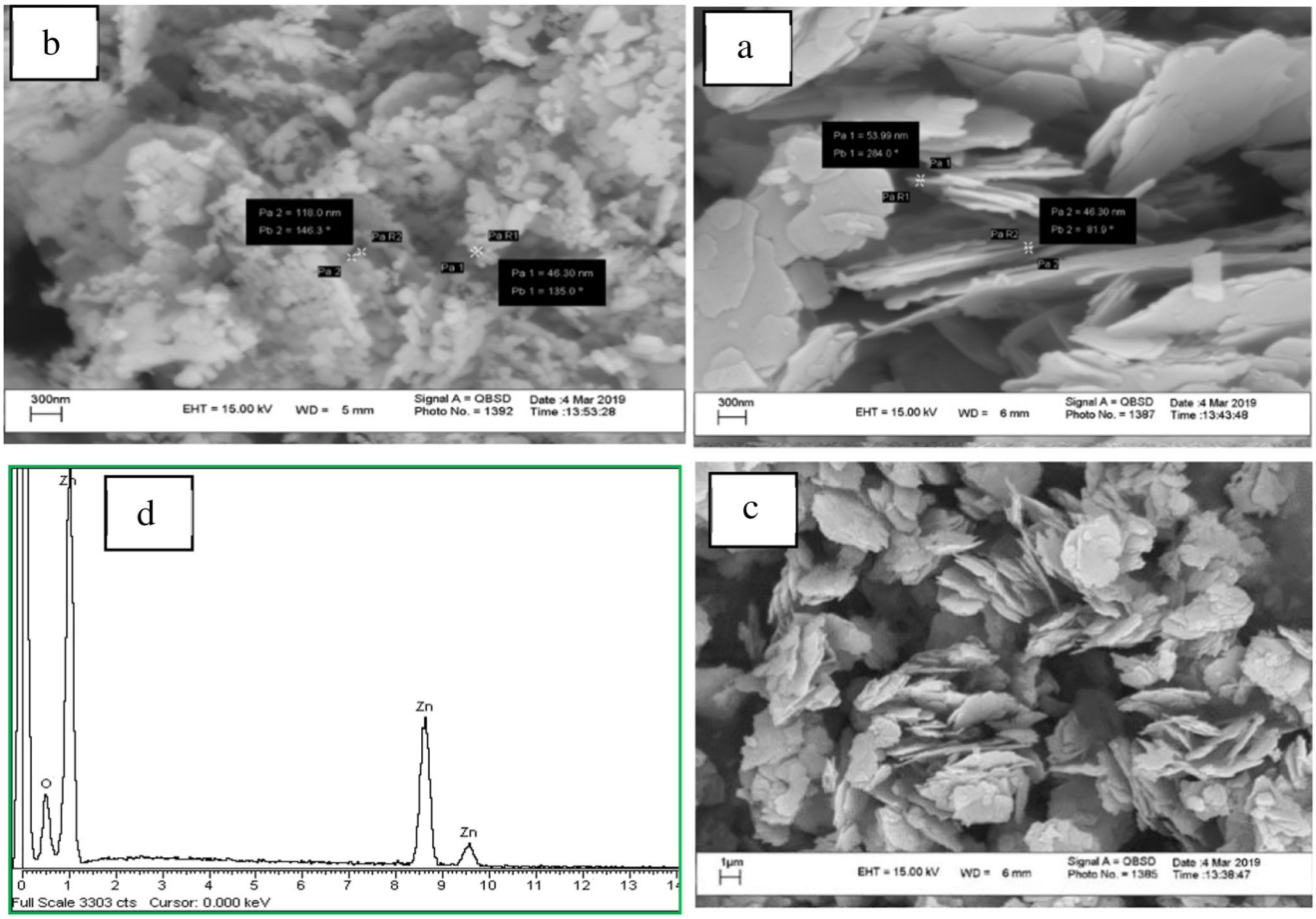

Fig. 6 SEM-EDS photomicrographs of precursor (**a**, **c**) and ZnO-nanoparticles (**b**) and EDS spectrum (**d**)

synthesized ZnO samples was 0.93 (Zn = 48.12%, O = 51.88%) compared to 4.086 in ideal ZnO stoichiometry implicating a 100% deviation in stoichiometric properties.

ICP-OES and wet chemical analysis confirmed the fabrication of high pure nano-ZnO (Table 4). There are still some minor impurities available (~1%) in the produced nanoparticles (e.g., iron, copper, nickel), which is negligible.

TEM micrographs in Fig. 7 confirm interconnections between the nanoparticles as already displayed in SEM results indicating the sintering influence of muffle-furnace calcination temperature at 850 °C [17]. A required number of TEM images are used to evaluate the nano-ZnO particle size distribution (PSD) linked with Image J software. The PSD with the average of 65±2 nm is estimated and shown for fabricated nano-ZnO in Fig. 7b. Agglomeration and electrostatic forces between the particles can explain the difference in average particle size determined by SEM and TEM [7, 8].

3.3.3 Crystallinity of ZnO-Nanoparticles

Figures 8 and 9 display the X-ray diffraction patterns of nano-ZnO precursor and ZnO nanoparticles while the ICDD standard specification numbers of 01-078-0246 and 01-075-1526 were extracted. The XRD pattern of well-crystalline nanoparticles (Fig. 9) presents hexagonal wurtzite-type ZnO with a lattice constant (a = 3.25 and c = 5.21 Å) with no diffraction peaks linked with impurities.

Table 4 ICP-OES and wet chemical analysis of produced ZnO nanoparticles

Composition	Concentration of the elements (%)
Zn	79.49
Fe	0.32
Cu	0.21
Cd	0.11
Ni	0.02
Ca	0.12
Na	0.11
Si*	0.04
S	0.10
Al	0.03
O	19.45

*Wet chemical method

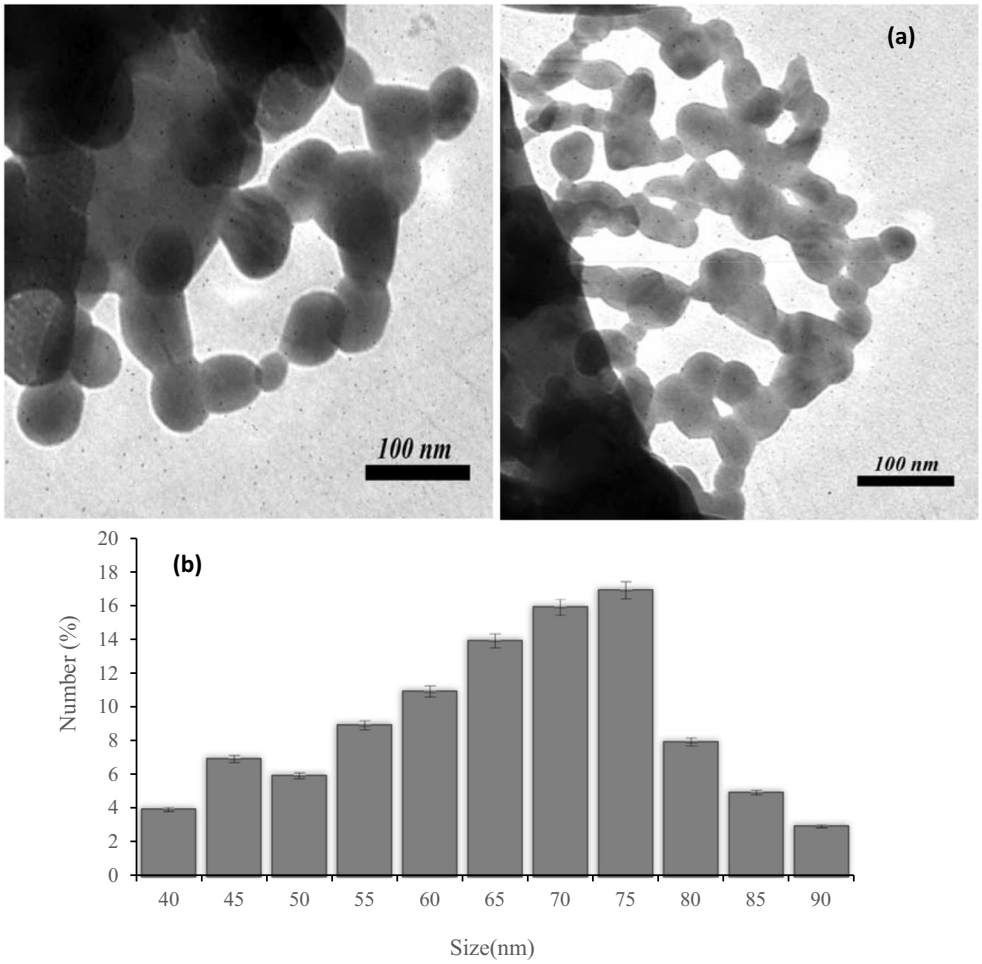

Fig. 7 As-synthesized ZnO-nanoparticles: **a** TEM images; **b** the PSD of the particles (mean size = 65 ± 2 nm)

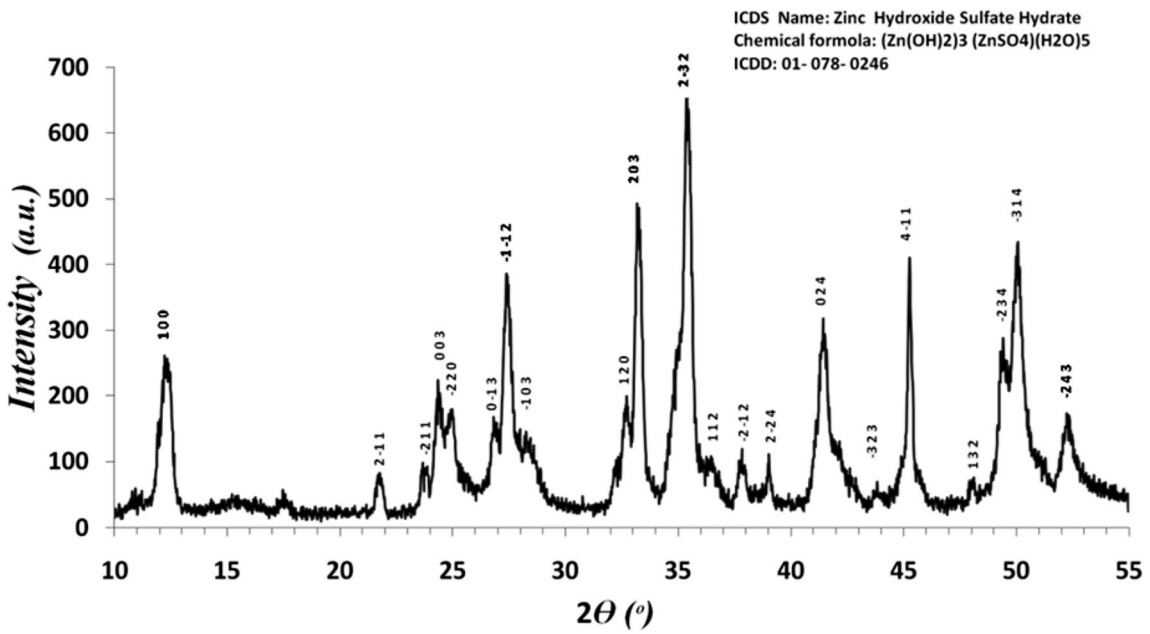

Fig. 8 XRD spectra of the as-prepared precursor

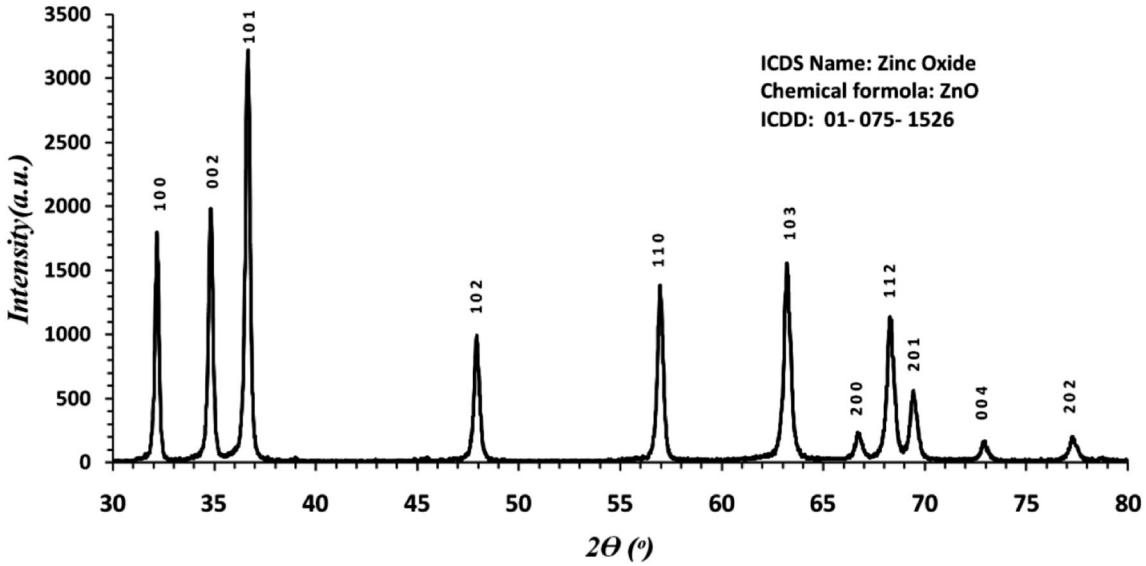

Fig. 9 XRD patterns of ZnO nanoparticles generated at 850 °C

When XRD patterns of precursor and nanoparticles were compared, it was found that the annealing process increased the crystallinity of the ZnO powder considerably by intensifying peak number 101 that implies the anisotropic growth and a preferred orientation of the crystallites [28]. The crystalline size (D) was evaluated by using Debye–Scherrer's formula presented in Eq. 4. K, λ, β, and θ represent grain shape factor, X-ray wavelength, corrected full width at half maximum value, and the angle at the maximum peak respectively (K=0.98, λ=0.15418 nm) [8]. The average theoretical crystallite size of the ZnO nanoparticles supposed to be 52 nm while in this study increased to more than 65 nm as the consequence of thermal treatment (Table 5).

$$D = K\,\lambda/\beta\cos\theta \tag{4}$$

3.3.4 Surface chemistry

Figure 10 compares the FTIR spectra of nano-ZnO precursor (A) and nano-ZnO (B). As displayed, most of the emerged peaks in the precursor were disappeared or the intensity was decreased in the nano-ZnO specimen that can be attributed to the thermal decomposition of the precursor. The emerged peaks at 448, 509, 601, 962, 1097, and 1122 cm^{-1} are stretch vibration bands of SO_4^{2-} ions present in mineralogical compositions of precursor while the stretching bands at 435 and 529 cm^{-1} present the vibration of Zn–O chemical bonds. The emerged peaks at 602, 693 cm^{-1} indicate the presence of Zn–OH bands present in the precursor sample [2, 6, 37].

The stretching bands at 1640, 3420, and 3446 cm^{-1} present the hydroxyl group and OH bending of water. The peaks at 2359, 2360 cm^{-1} imply the existence of the CO_2 stretch vibration band [2, 5–7, 37]. The functional OH groups, CO_2, and the Zn–O metal bonding group can be considered as another strong reason for the high purity of the ZnO product since the presence of even very small traces of impurities shows themself as the characteristic peaks in the FTIR analysis.

4 Conclusion

The generation of nano-ZnO from EAFD was accomplished in this study using a hydrometallurgical method. The purification of acid leached EAFD was achieved using sodium hydroxide and di-2 ethylhexyl phosphoric acid reagents. Preparation of $(Zn(OH)_2)_3(ZnSO_4)(H_2O)_5$ as the precursor of nano-ZnO was completed by dropping ammonium hydroxide to purified PLS solution while the fabrication of nano-ZnO

Table 5 X-ray powder diffraction data and the estimated size of crystallites diffraction peaks

h	k	l	$d_{cal.}$	$d_{meas.}$	Crystallite size (A°)
1	0	0	2.7886	2.7880	573
0	0	2	2.6000	2.5957	512
1	0	1	2.4575	2.4555	356
1	0	2	1.9016	1.8985	601
1	1	0	1.6100	1.6162	860
1	0	3	1.4721	1.4710	292
2	0	0	1.3943	1.4011	531
1	1	2	1.3688	1.3712	594
2	0	1	1.3467	1.3539	455
0	0	4	1.3000	1.2976	704
2	0	2	1.2287	1.2348	388

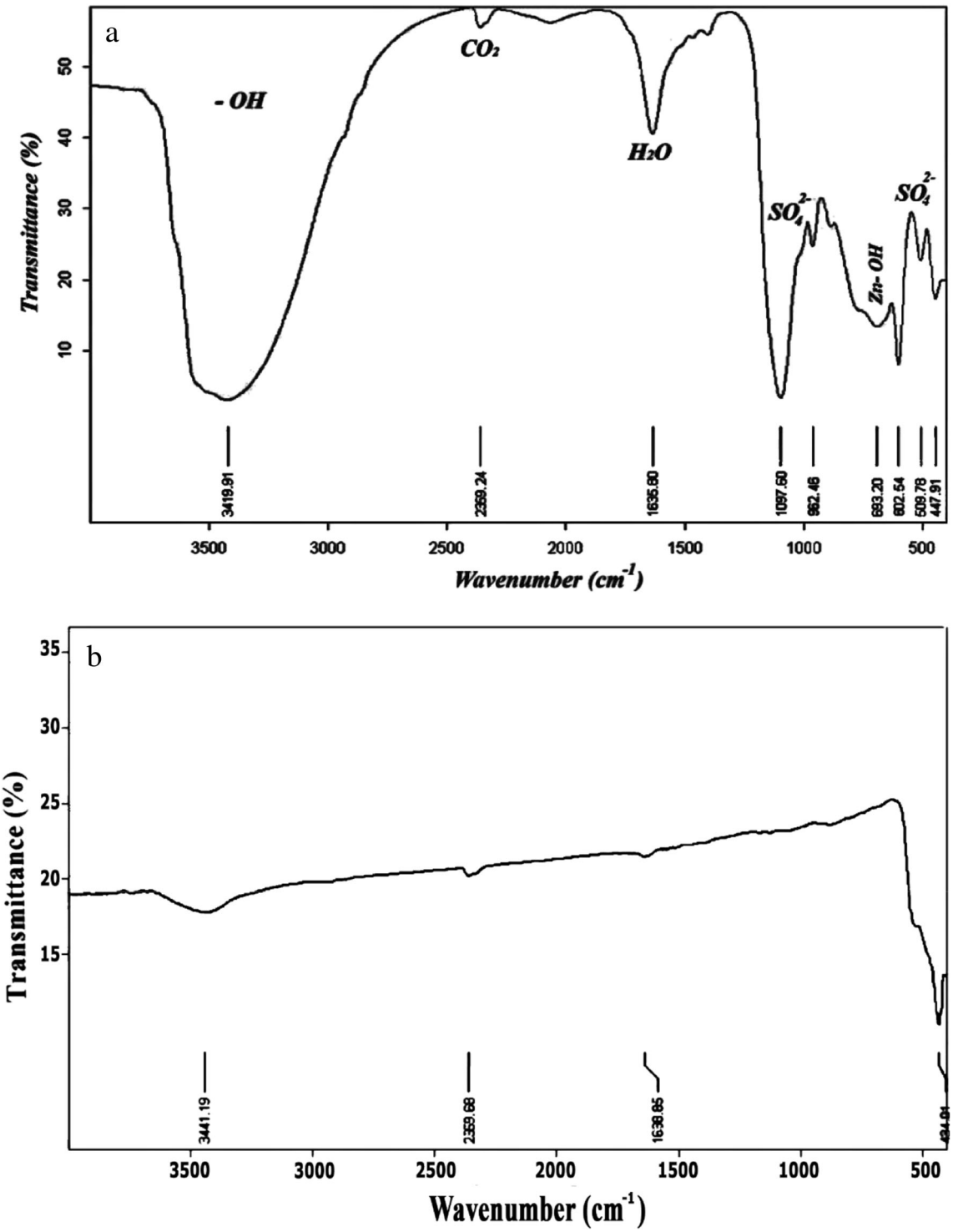

Fig. 10 The FTIR spectra of **a** precursor and **b** ZnO nanoparticles

was conducted using the thermal treatment on the precursor. Since iron oxide is a major component in EAFD that freely releases to PLS, it is worthy to consider simultaneous fabrication of nano iron oxide during the synthesis of nano-ZnO to decrease the cost of operation by the addition of another value-added product.

Acknowledgements This work was financially supported by the IRANIAN National science foundation (No. 90003855). We also want to appreciate the cooperation of Dr. Ali Khodayari from the SEM/EDS analysis unit of University of Mohaghegh Ardabili.

Declarations

Conflict of Interest On behalf of all authors, the corresponding author states that there is no conflict of interest.

References

1. Baba AA, Adekola FA (2011) Beneficiation of a Nigerian sphalerite mineral: solvent extraction of zinc by Cyanex® 272 in hydrochloric acid. Hydrometallurgy 109:187–193
2. Bakhtiari F, Darezereshki E (2011) One-step synthesis of tenorite (CuO) nano-particles from Cu4 (SO4)(OH) 6 by direct thermal-decomposition method. Mater Lett 65:171–174
3. Brunelli K, Dabalà M (2015) Ultrasound effects on zinc recovery from EAF dust by sulfuric acid leaching. Int J Miner Metall Mater 22:353–362
4. Cashman JB (1998) Hydrometallurgical processing of flue dust. In: Google Patents. Patent No. US005709730A: 1-9
5. Darezereshki E (2010) Synthesis of maghemite (γ-Fe_2O_3) nanoparticles by wet chemical method at room temperature. Mater Lett 64: 1471–1472
6. Darezereshki E, Alizadeh M, Bakhtiari F, Schaffie M, Ranjbar M (2011) A novel thermal decomposition method for the synthesis of ZnO nanoparticles from low concentration $ZnSO_4$ solutions. Appl Clay Sci 54:107–111
7. Darezereshki E, Bakhtiari F, Alizadeh M, Ranjbar M (2012) Direct thermal decomposition synthesis and characterization of hematite (α-Fe_2O_3) nanoparticles. Mater Sci Semicond Process 15:91–97
8. Darezereshki E, Ranjbar M, Bakhtiari F (2010) One-step synthesis of maghemite (γ-Fe_2O_3) nano-particles by wet chemical method. J Alloys Compd 502:257–260
9. Geetha D, Thilagavathi T (2010) Hydrothermal synthesis of nano ZnO structures from CTAB. Dig J Nanomater Biostruct 5:297–301
10. Halli P, Hamuyuni J, Leikola M, Lundström M (2018) Developing a sustainable solution for recycling electric arc furnace dust via organic acid leaching. Miner Eng 124:1–9
11. Halli P, Hamuyuni J, Revitzer H, Lundström M (2017) Selection of leaching media for metal dissolution from electric arc furnace dust. J Clean Prod 164:265–276
12. Hammad TM, Salem JK, Harrison RG (2009) Synthesis, characterization, and optical properties of Y-doped ZnO nanoparticles. Nano 4:225–232
13. Hasnidawani JN, Azlina HN, Norita H, Bonnia NN, Ratim S, Ali ES (2016) Synthesis of ZnO nanostructures using sol-gel method. Procedia Chem 19:211–216
14. Havlik T, Turzakova M, Stopic S, Friedrich B (2005) Atmospheric leaching of EAF dust with diluted sulphuric acid. Hydrometallurgy 77:41–50
15. Jha MK, Kumar V, Singh RJ (2001) Review of hydrometallurgical recovery of zinc from industrial wastes. Resour Conserv Recycl 33: 1–22
16. Koohestani B, Darban AK, Darezereshki E, Mokhtari P, Yilmaz E, Yilmaz E (2018) The influence of sodium and sulfate ions on total solidification and encapsulation potential of iron-rich acid mine drainage in silica gel. J Environ Chem Eng 6:3520–3527
17. Koohestani B, Darban AK, Mokhtari P, Darezereshki E, Yilmaz E, Yilmaz E (2020) Influence of hydrofluoric acid leaching and roasting on mineralogical phase transformation of pyrite in sulfidic mine tailings. Minerals 10:513
18. Kurama H, Çatalsarik T (2000) Removal of zinc cyanide from a leach solution by an anionic ion-exchange resin. Desalination 129: 1–6
19. Leclerc N, Meux E, Lecuire J-M (2002) Hydrometallurgical recovery of zinc and lead from electric arc furnace dust using mononitrilotriacetate anion and hexahydrated ferric chloride. J Hazard Mater 91:257–270
20. Li X, Monnens W, Zheng L, Fransaer J, Binnemans K (2020) Solvometallurgical process for extraction of copper from chalcopyrite and other sulfidic ore minerals. Green Chem 22:417–426
21. Liang JZ (2020) Melt Elongation Flow Behavior of Low-Density Polyethylene Composites Filled with Nanoscale Zinc Oxide. J Test Eval 48:4551–4562
22. Lin X, Peng Z, Yan J, Li Z, Hwang J-Y, Zhang Y, Li G, Jiang T (2017) Pyrometallurgical recycling of electric arc furnace dust. J Clean Prod 149:1079–1100
23. Lis T, Nowacki K, Żelichowska M, Kania H (2015) Innovation in metallurgical waste management. Metalurgija 54:283–285
24. Machado JGMS, Brehm FA, Moraes CAM, Santos CAD, Vilela ACF, Da Cunha JBM (2006) Chemical, physical, structural and morphological characterization of the electric arc furnace dust. J Hazard Mater 136:953–960
25. Madhi A, Hadavand BS (2020) Eco-friendly castor oil-based UV-curable urethane acrylate zinc oxide nanocomposites: synthesis and viscoelastic behavior. J Compos Mater 54:101–110
26. Maweja K, Mukongo T, Mbaya RK, Mochubele EA (2010) Effect of annealing treatment on the crystallisation and leaching of dumped base metal smelter slags. J Hazard Mater 183:294–300
27. Montenegro V, Oustadakis P, Tsakiridis PE, Agatzini-Leonardou S (2013) Hydrometallurgical treatment of steelmaking electric arc furnace dusts (EAFD). Metall Mater Trans B 44:1058–1069
28. Muruganandham M, Chen IS, Wu JJ (2009) Effect of temperature on the formation of macroporous ZnO bundles and its application in photocatalysis. J Hazard Mater 172:700–706
29. Niubó M, Fernández AI, Chimenos JM, Haurie L (2009) A possible recycling method for high grade steels EAFD in polymer composites. J Hazard Mater 171:1139–1144
30. Omran M, Fabritius T, Heikkinen E-P (2019) Selective Zinc Removal from Electric Arc Furnace (EAF) Dust by Using Microwave Heating. J Sustain Metall 5:331–340
31. Oustadakis P, Tsakiridis PE, Katsiapi A, Agatzini-Leonardou S (2010) Hydrometallurgical process for zinc recovery from electric arc furnace dust (EAFD): Part I: Characterization and leaching by diluted sulphuric acid. J Hazard Mater 179:1–7
32. Pickles CA (2010) Thermodynamic modelling of the formation of zinc–manganese ferrite spinel in electric arc furnace dust. J Hazard Mater 179:309–317
33. Ruiz O, Clemente C, Alonso M, Alguacil FJ (2007) Recycling of an electric arc furnace flue dust to obtain high grade ZnO. J Hazard Mater 141:33–36
34. Spanhel L (2006) Colloidal ZnO nanostructures and functional coatings: a survey. J Sol-Gel Sci Technol 39:7–24
35. Tsakiridis PE, Oustadakis P, Katsiapi A, Agatzini-Leonardou S (2010) Hydrometallurgical process for zinc recovery from electric arc furnace dust (EAFD). Part II: Downstream processing and zinc recovery by electrowinning. J Hazard Mater 179:8–14
36. Vakylabad AB (2011) A comparison of bioleaching ability of mesophilic and moderately thermophilic culture on copper bioleaching from flotation concentrate and smelter dust. Int J Miner Process 101:94–99
37. Vakylabad AB, Schaffie M, Naseri A, Ranjbar M, Manafi Z (2016) A procedure for processing of pregnant leach solution (PLS) produced from a chalcopyrite-ore bio-heap: CuO Nano-powder fabrication. Hydrometallurgy 163:24–32

38. Wang H-g, Yang L, Gao J-m, Zhang M, Guo M (2016) A novel hydrothermal method for zinc extraction and separation from zinc ferrite and electric arc furnace dust. Int J Miner Metall Mater 23: 146–155
39. Weiβ Th, Xalter R (2014) Nano silver-zinc oxide composition. In: Google Patents. Patent No. US008951543B2: 1-11
40. Woolard CD, Williams DC, Van Rooyen JL, Garde K, Bosch RM, Strydom SHJ (2013) Non-polar capped nano transition metal oxides and sulfides. In: Google Patents. Patent No. US20100305332A1: 1-9.
41. Xanthopoulos P, Agatzini-Leonardou S, Oustadakis P, Tsakiridis PE (2017) Zinc recovery from purified electric arc furnace dust leach liquors by chemical precipitation. J Environ Chem Eng 5: 3550–3559
42. Ye Q, Peng Z, Li G, Lee J, Liu Y, Liu M, Wang L, Rao M, Zhang Y, Jiang T (2019) Microwave-assisted reduction of electric arc furnace dust with biochar: an examination of transition of heating mechanism. ACS Sustain Chem Eng 7:9515–9524
43. Yu B-S, Wang Y-R, Chang T-C (2011) Hydrothermal treatment of electric arc furnace dust. J Hazard Mater 190:397–402
44. Zhan L, Li O, Zhenming X (2020) Preparing nano-zinc oxide with high-added-value from waste zinc manganese battery by vacuum evaporation and oxygen-control oxidation. J Clean Prod 251: 119691
45. Zhang Y, Zhang Y, Zhang S, Yang G, Gao C, Zhou C, Zhang C, Zhang P (2020) One step synthesis of ZnO nanoparticles from ZDDP and its tribological properties in steel-aluminum contacts. Tribol Int 141:105890